Journal of NAMP 73 (2026) 23-34

The Nigerian Association of Mathematical Physics

Journal homepage: https://nampjournals.org.ng

Unified Optical Dispersion Modelling of Perovskite Solar Cells

Hassan Abdulsalam[1]*, Habiba Garba Ahmad[2], Mohammed Bukar Dapchi[1], and Hassana Muhammad Shuwa[1]

[1]*Department of Physics, Yobe State University, P.M.B. 1144, Damaturu, Yobe State, Nigeria*

[2]*Physics Department, Yusuf Maitama Sule Federal University of Education, Kano,*

***Corresponding Author**: ahassanabdulsalam@gmail.com **;** +234 8068061599

ARTICLE INFO

Article history:
Received xxxxx
Revised xxxxx
Accepted xxxxx
Available online xxxxx

Keywords:
Perovskite solar cells,
Refractive index dispersion,
Extinction coefficient,
Sellmeier model,
Thermo-optic effects,
Lorentz oscillator model.

ABSTRACT

This work presents a unified optical dispersion framework for perovskite solar cell materials that incorporates wavelength- and temperature-dependent effects. The refractive index was modeled using a two-oscillator Sellmeier equation combined with a thermo-optic polynomial to describe variations with photon energy and temperature. Optical absorption was represented using the Lorentz damped harmonic oscillator model, providing a physically consistent description of extinction spectra. Validation against experimental data spanning 298.15–348.15 K and band gaps of 1.58–1.77 eV showed excellent agreement. The Sellmeier model achieved near-perfect fits ($R2 \approx 0.99999$), the thermo-optic extension provided unified predictions ($R2 \approx 0.866$), and the Lorentz model reproduced extinction behavior with R^2 values up to 0.99. The results demonstrate strong coupling between thermal effects, electronic transitions, and optical dispersion. This framework bridges material characterization and device-level simulation, enabling improved prediction of perovskite solar cell performance, thermal stability, and energy yield under realistic operating conditions.

1. Introduction

Perovskite solar cells (PSCs) have emerged as one of the most promising photovoltaic technologies due to their exceptional optoelectronic properties, low-cost fabrication, and power conversion efficiencies exceeding 26%[1]. Their rapid development is driven by strong optical absorption, tuneable bandgaps, long carrier diffusion lengths, and efficient charge transport, making PSCs attractive candidates for next-generation solar energy conversion [2, 3].

*Corresponding author: **Hassan Abdulsalam**, (+234 8068061599)

E-mail address: ahassanabdulsalam@gmail.com

DOI: https://doi.org/10.60787/tnamp.v25.715

1118-4388 © 2024 JNAMP. All rights reserved

Accurate knowledge of the optical constants, namely the refractive index (n) and extinction coefficient (k), is essential for understanding and optimizing PSC performance. These parameters govern light propagation, reflection, absorption, and interference within the device, directly influencing photon harvesting and charge-carrier generation. In perovskite materials, both n and k exhibit strong wavelength dependence and are further affected by temperature through lattice expansion, electron–phonon interactions, and changes in electronic band structure[4]. Consequently, reliable optical models must account for both spectral and thermal effects.

The Sellmeier equation provides a well-established framework for describing refractive-index dispersion and has been successfully applied to a wide range of optical materials, including semiconductors and hybrid perovskites[5]. By representing wavelength-dependent behaviour with a small set of physically meaningful parameters, it offers an efficient approach for modelling refractive-index spectra across the visible and near-infrared regions. For absorption-related properties, physically based dispersion models are required to capture the complex behaviour of the extinction coefficient. In hybrid perovskites, optical absorption is dominated by inter-band electronic transitions near the direct bandgap and is strongly influenced by temperature-dependent bandgap shifts and spectral broadening[6, 7].

Among the available approaches, the Lorentz oscillator formalism provides a physically consistent description of optical absorption by representing electronic transitions as damped resonant oscillators. Combined with thermo-optic corrections, such models enable accurate characterization of temperature-dependent optical responses and facilitate advanced optoelectronic analysis. These modelling strategies have been widely employed in the study of semiconductors and emerging photovoltaic materials[8-11].

Despite extensive optical characterization of perovskite materials, many studies continue to rely on room-temperature optical constants or neglect explicit thermal effects in spectral modelling. Such simplifications can limit predictive accuracy because PSCs often operate at temperatures significantly above ambient conditions, where changes in n and k alter light absorption and carrier-generation profiles. Furthermore, while first-principles methods can capture these effects, they are frequently computationally demanding for routine device-level simulations.

To address these challenges, this work develops a unified optical dispersion framework for perovskite solar cells by integrating Sellmeier-based refractive-index dispersion, thermo-optic corrections, and Lorentz-based absorption modelling. The framework is validated using temperature-dependent datasets spanning 25–75 °C (298.15–348.15 K) and band gaps between 1.58 and 1.77 eV[12]. By simultaneously accounting for spectral and thermal effects, the proposed model provides a computationally efficient and physically grounded tool for optical characterization, device simulation, and the prediction of PSC performance under realistic operating conditions.

2. THEORETICAL BACKGROUND

2.1 Optical Behaviour of Perovskite Solar Cell Materials

2.1.1 Complex Refractive Index

The optical response of perovskite solar cell materials is described by the complex refractive index:

$$\tilde{n}(\lambda, T) = n(\lambda, T) + ik(\lambda, T) \qquad (1)$$

where n(λ,T) is the refractive index associated with phase velocity and k(λ,T) is the extinction coefficient governing optical absorption. Both quantities depend on wavelength and temperature due to variations in electronic structure, lattice vibrations, and electron–phonon interactions[2, 13]. Accurate determination of n and k is essential because they control light propagation, reflection, interference, and absorption within photovoltaic devices.

2.1.2 The Sellmeier Dispersion Model

For spectral regions where absorption is negligible, the extinction coefficient approaches zero:

$$k(\lambda) \approx 0 \qquad (2)$$

and the complex refractive index reduces to

$$\tilde{n}(\lambda, T) \approx n(\lambda, T) \qquad (3)$$

Under this assumption, optical behaviour is dominated by dielectric polarization arising from bound electronic oscillations. The refractive-index dispersion can therefore be represented using the two-oscillator Sellmeier equation:

$$n^2(\lambda) = 1 + \frac{B_1\lambda^2}{\lambda^2 - C_1} + \frac{B_2\lambda^2}{\lambda^2 - C_2} \qquad (4)$$

where B_1 and B_2 denote oscillator strengths, while C_1 and C_2 represent resonance wavelength constants associated with electronic transitions. The Sellmeier model provides an efficient and physically meaningful description of refractive-index dispersion and has been widely applied to semiconductors, dielectric materials, and hybrid perovskites[14]. Its suitability for perovskite materials arises from its ability to capture wavelength-dependent optical behaviour across the visible and near-infrared spectral regions.

2.1.3 Thermo-Optic Extension

Because perovskite optical properties vary with temperature, the Sellmeier model can be extended through a thermo-optic correction:

$$n(\lambda, T, E) = n(\lambda, T_0) + (a_0 + a_1\lambda + a_2\lambda^2 + b_1E + b_2E^2 + c\lambda E)(T - T_0) \quad (5)$$

where $n(\lambda,T_0)$ is the refractive index at a reference temperature T_0. The polynomial term approximates the thermo-optic coefficient dn/dT as a function of wavelength and photon energy. This extension enables simultaneous representation of intrinsic dispersion, thermal effects, and near-band-edge variations within a unified framework. Similar approaches have demonstrated strong predictive capability for both crystalline and amorphous optical materials [10, 11].

2.2 Complex Dielectric Response and Optical Absorption

The interaction of electromagnetic radiation with a semiconductor is fundamentally governed by the complex dielectric function:

$$\tilde{\varepsilon}(E) = \varepsilon_1(E) + i\varepsilon_2(E) \qquad (6)$$

where E = hc/λ is the photon energy. The real component ε_1 describes dispersion and phase propagation, whereas the imaginary component ε_2 accounts for optical losses resulting from electronic transitions and absorption processes[14, 15]. In direct-bandgap perovskites, the dielectric response near the absorption edge is dominated by inter-band transitions, making dielectric-function-based models particularly useful for describing optical absorption.

2.2.1 Lorentz Damped Harmonic Oscillator Formalism

To model absorption processes, bound electrons may be treated as damped harmonic oscillators driven by an incident electromagnetic field. The resulting Lorentz oscillator model provides a

physically consistent description of resonant optical transitions and satisfies causality through the Kramers–Kronig relations. For a material containing j dominant electronic transitions, the dielectric function is expressed as:

$$\tilde{\varepsilon}(E) = \varepsilon_\infty + \sum_j \frac{f_j}{E_{0,j}^2 - E^2 - i\gamma_j E} \qquad (7)$$

where ε_∞ is the high-frequency dielectric constant, f_j is the oscillator strength, $E_{o,j}$ is the resonance energy, and γ_j is the damping parameter. The oscillator strength determines the intensity of a transition, whereas the damping parameter controls spectral broadening and is related to carrier-scattering processes.

In perovskite materials, γ_j is strongly influenced by electron–phonon interactions, dynamic lattice disorder, and defect scattering. Consequently, temperature variations modify resonance linewidths and absorption spectra, making the Lorentz formalism particularly suitable for describing thermally induced optical broadening[16, 17]. The model therefore provides a direct link between measured optical spectra and the underlying electronic structure of the material.

2.2.2 Derivation of the Extinction Coefficient

The complex refractive index and dielectric function are related through: $\tilde{n}^2 = \tilde{\varepsilon}$ [14, 18]. Using this relationship, the extinction coefficient may be obtained from the imaginary component of the dielectric response:

$$k(E) = Im\left[\sqrt{\tilde{\varepsilon}(E)}\right] = \sqrt{\frac{\sqrt{\varepsilon_1^2(E) + \varepsilon_2^2(E)} - \varepsilon_1(E)}{2}} \qquad (8)$$

This expression guarantees physically meaningful solutions with $k \geq 0$ and avoids numerical ambiguities associated with direct evaluation of complex square roots. Near the optical band edge, the extinction coefficient reflects the onset of inter-band absorption and provides valuable information regarding electronic transitions, disorder effects, and absorption broadening. Oscillator-based models such as the Lorentz formalism therefore offer a reliable framework for reproducing experimentally observed extinction spectra.

2.2.3 Relevance to Perovskite Optical Modelling

A major advantage of the Lorentz oscillator model is that its parameters possess direct physical significance. Unlike purely empirical dispersion relations, the resonance energy, damping coefficient, oscillator strength, and dielectric constant can be related to fundamental material properties and their temperature dependence[14, 18]. In halide perovskites, these parameters enable characterization of bandgap evolution, spectral broadening, and dielectric behaviour from experimentally measured optical spectra.

The combination of Sellmeier dispersion, thermo-optic corrections, and Lorentz absorption modeling provides a comprehensive framework for describing both refractive and absorptive optical processes. When coupled with nonlinear regression and constrained optimization techniques, these models yield robust parameter extraction and reliable predictive capability across the spectral range relevant to photovoltaic applications. Consequently, they form the theoretical basis for temperature-dependent optical characterization and device-level simulation of perovskite solar cells.

3. MATERIALS AND METHODS

3.1 Data Source and Description

The dataset used in this study was obtained from spectroscopic ellipsometry measurements on triple-cation perovskite solar cells (PSCs) [12]. It contains wavelength-dependent refractive index n(λ,T) and extinction coefficient k(λ,T) measured over temperatures from 25–75 °C and band gaps ranging from 1.58–1.77 eV.

The dataset captures near-band-edge optical behavior in perovskite thin films, where electronic transitions and temperature-dependent lattice effects significantly influence optical response. The simultaneous spectral and thermal resolution makes the dataset suitable for dispersion modeling and thermo-optic analysis under realistic operating conditions.

The data were used exclusively for numerical modeling and parameter extraction. All usage complied with an ACS RightsLink license (License No. 6264710405703, issued May 09, 2026), permitting academic reuse.

3.2 Data Pre-processing

The dataset consisted of n(λ,T) and k(λ,T) values across five band gaps (1.58–1.77 eV) and six temperature points (298.15–348.15 K), giving 30 total experimental conditions.

Temperature values were standardized to Kelvin and organized into structured arrays for regression analysis. For refractive-index modeling, only spectral regions with negligible absorption ($k \approx 0$) were used. For extinction modeling, full k(λ,T) datasets were retained to preserve absorption features.

Photon energy was computed using: $E = hc/\lambda$ where h is Planck's constant and c is the speed of light. The dataset was reformatted into two modelling domains: (λ, T, n) for dispersion analysis and (E, T, k) for dielectric-function modeling. This ensured consistency between physical variables and model formulation.

3.3 Sellmeier Dispersion and Thermo-Optic Modeling

3.3.1 Sellmeier Model

The refractive index dispersion was modeled using the two-term Sellmeier equation (Equation 4). The model assumes weak absorption ($k \approx 0$), making it valid in transparency regions away from the absorption edge. Parameters were estimated using nonlinear least-squares regression via the Levenberg–Marquardt algorithm (nlsLM, R package minpack.lm). Initial guesses were selected based on literature-reported perovskite optical constants, and constraints ($0.01 \leq B_i \leq 10$, $10^{-6} \leq C_i \leq 1\ \mu m^2$) were applied to ensure physically meaningful solutions.

Model accuracy was assessed using coefficient of determination (R^2) and root mean square error (RMSE), computed on n^2 values to preserve linearity of the Sellmeier formulation.

3.3.2 Thermo-Optic Extension

To incorporate temperature and photon-energy dependence, the extended Sellmeier model was used (Equation 5). All parameters were estimated simultaneously using multiple linear regression (lm in R), ensuring coupled optimization across all variables and preserving parameter covariance. This unified fitting avoids error accumulation associated with sequential calibration. The extended model captures intrinsic dispersion, thermal variation, and near-band-edge perturbations within a single analytical framework suitable for device-level simulation.

3.4 Lorentz Oscillator Model for Extinction Coefficient

Prior to modeling, a unit-consistency check was performed on k(λ,T). When extinction values exceeded 5, they were interpreted as absorption coefficients (α in cm^{-1}) and converted using: $k = \alpha\lambda \times 10^{-7}/4\pi$, ensuring dimensional consistency with the Lorentz formalism. The dielectric response was modeled using the Lorentz oscillator (Equation 7).

Temperature dependence was introduced by allowing $E_{0,j}(T)$ to vary linearly and $\gamma_j(T)$ to vary quadratically, capturing bandgap renormalization and thermally induced spectral broadening.

The extinction coefficient was obtained using Equation 8, this formulation ensures numerical stability and guarantees $k \geq 0$ across the spectral domain.

A two-stage fitting strategy was applied. First, a single-oscillator model was initialized using peak estimation $E_0 \approx hc/\lambda_{max}$. Second, a two-oscillator model was fitted, where the additional oscillator accounts for higher-energy interband transitions and excitonic shoulders.

3.5 Computational Framework and Validation

All computations were implemented in R (v4.3+). The workflow included automated data preprocessing, nonlinear regression, parameter estimation, and validation.

Wavelength data were converted from nm to μm for Sellmeier consistency, while photon energy was used for dielectric-function modeling. Batch processing ensured consistent application across all temperature and bandgap conditions.

Model performance was evaluated using:

$$R^2 = 1 - \frac{\sum\left(Y_{exp} - Y_{model}\right)^2}{\sum\left(Y_{exp} - \bar{Y}_{exp}\right)^2} \qquad (9)$$

$$RMSE = \sqrt{\frac{1}{N}\sum\left(Y_{exp} - Y_{model}\right)^2} \qquad (10)$$

where Y_{exp} and Y_{model} are experimental and predicted values, and N is the number of observations.

Validation included both statistical and graphical assessments. Residual analysis was performed to detect systematic deviations, particularly near the absorption edge where optical transitions are highly sensitive to parameter variations. Agreement between modeled and experimental spectra was confirmed across all temperatures and band gaps.

The complete workflow was fully automated to ensure reproducibility. This includes dataset ingestion, parameter optimization, and visualization. The integrated framework enables consistent extraction of physically meaningful optical parameters and supports predictive modeling of temperature-dependent optical behavior in perovskite solar cells.

4. RESULTS AND DISCUSSION

4.1 Sellmeier Modelling of Wavelength-Dependent Refractive Index

Table 1 summarizes the extracted Sellmeier coefficients under different temperature and bandgap conditions. The model demonstrates excellent agreement with experimental data, with R^2 values between 0.999968 and 0.999990 and RMSE on the order of 10^{-3}, confirming high numerical stability within the transparent spectral region [19].

The oscillator strength B_1 decreases with increasing temperature, indicating reduced contribution from low-energy electronic transitions due to lattice expansion and enhanced electron–phonon

interactions[13]. In contrast, B_2 shows a slight increase, suggesting enhanced higher-energy polarization contributions. The resonance parameters C_1 and C_2 vary non-monotonically with temperature, reflecting thermally induced band structure renormalization and redistribution of optical transition strength[7, 20]. These trends confirm strong coupling between thermal and electronic effects in dispersion behaviour.

Table 1 Sellmeier coefficients obtained under different photon-energy and temperature conditions

Conditions		Sellmeier Coefficients				Fit Quality Parameters	
Band gap (eV)	**Temperature (c)**	**B_1**	**C_1 (μm²)**	**B2**	**C^2 (μm²)**	**R^2**	**RMSE**
1.58	298.15	4.040758	0.108388	0.160932	0.537215	0.999990	0.000984
1.66	308.15	3.909199	0.096038	0.156261	0.484258	0.999971	0.001797
1.68	318.15	3.789550	0.098817	0.154746	0.469887	0.999968	0.001889
1.71	328.15	3.653562	0.097603	0.156869	0.451533	0.999981	0.001413
1.77	338.15	3.662714	0.075884	0.202360	0.411161	0.999986	0.001070
	348.15	3.639574	0.075074	0.215230	0.403692	0.999990	0.000886

4.2 Unified Thermo-Optic Model and Statistical Validation

To generalize dispersion behaviour, a unified thermo-optic model (Eq. 5) was applied across all wavelengths, temperatures, and bandgaps. The model achieved R^2 = 0.8661 and RMSE = 0.0272 across 12,188 observations (Table 2). While lower than condition-specific Sellmeier fits, this reflects the increased dimensional complexity and single-equation constraint. The baseline refractive index function exhibits nonlinear dispersion consistent with semiconductor optical response. The negative linear wavelength term and positive quadratic contribution indicate normal dispersion with curvature enhancement at shorter wavelengths. The thermo-optic correction term captures coupled dependence on wavelength, photon energy, and temperature. The interaction term (λE) confirms that thermal response cannot be separated from spectral and electronic effects, highlighting intrinsic coupling in perovskite optical behaviour.

Table 2 Thermo-optic refractive index model fit parameters and statistical performance

Section	Metric / Coefficient	Value
Reference	Temp (T_0)	298.15 K
	Total Observations	12,188
Baseline Model $n(\lambda, T_0)$ $n(\lambda, T_0) = d_0 + d_1 \cdot \lambda + d_2 \cdot \lambda^2$	d_0 (Intercept)	3.10122
	d_1	-1.10678
	d_2	0.37206
Temp-Dependent $\Delta n = (a_0 + a_1\lambda + a_2\lambda^2 + b_1E + b_2E^2 + c\lambda E) \cdot (T - T_0)$	a_0 (constant)	0.18778
	a_1	-0.01581
	a_2	-0.00014
	b_1	-0.19697
	b_2	0.05053
	c	0.00954

4.3 Model Performance Evaluation and Comparative Analysis

Figure 1 presents refractive index variation with wavelength across different temperatures and bandgaps. Table 3 compares RMSE values for Sellmeier and thermo-optic models.

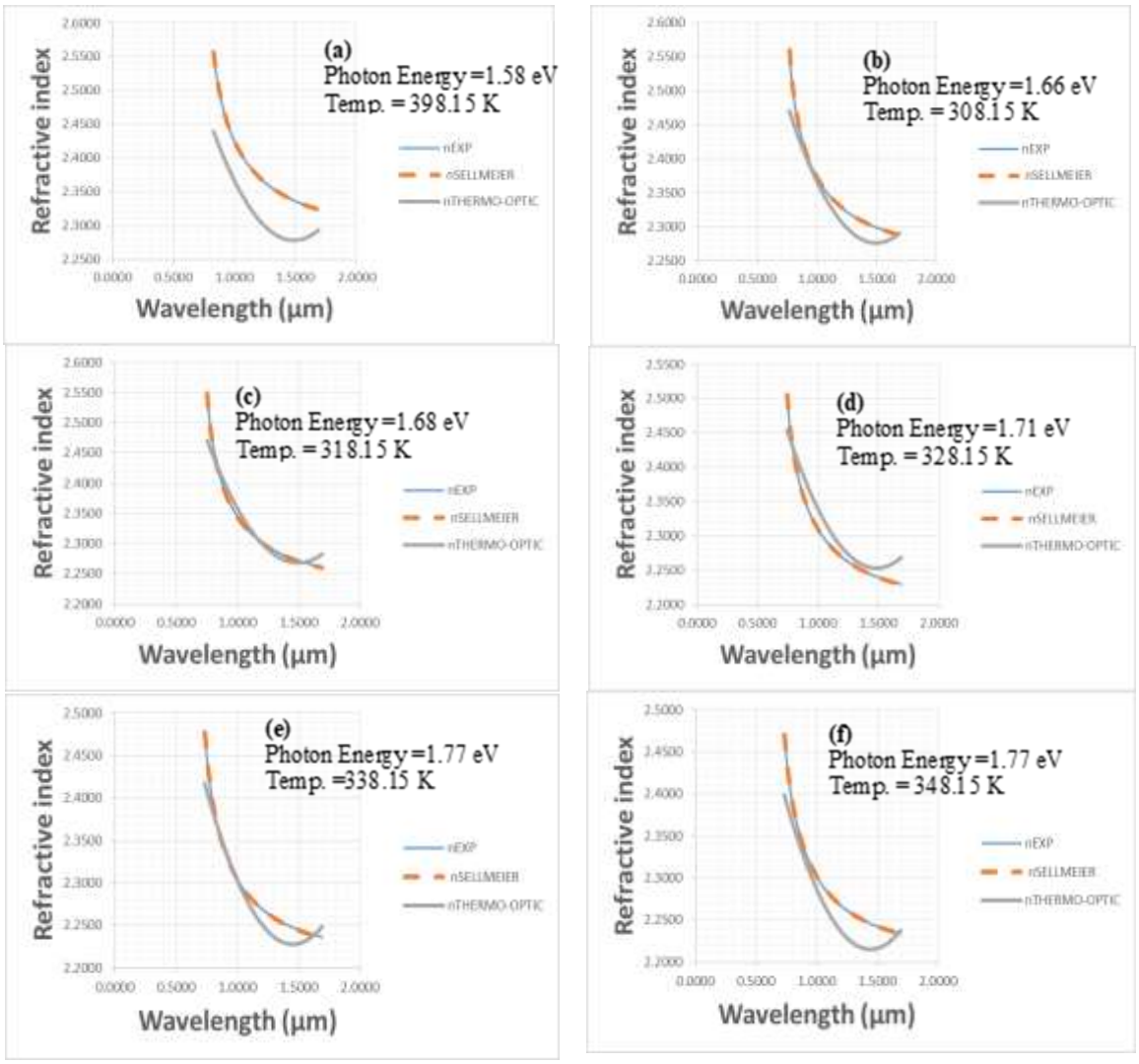

Figure 1 Wavelength-dependent refractive index variation predicted by the Sellmeier and thermo-optic models at different photon energies and temperatures

The Sellmeier model consistently achieves lower RMSE (10^{-3} range), indicating superior accuracy for condition-specific fitting. However, it requires independent parameterization for each condition. In contrast, the thermo-optic model provides a unified predictive framework across all conditions. Although less accurate, it significantly improves scalability and reduces redundancy, highlighting a trade-off between precision and generalization.

Table 3 Root mean square error comparison of Sellmeier and thermo-optic models across selected band gap and temperature conditions

Conditions		RMSE	
Band gap (eV)	**Temperature (K)**	**Sellmeier**	**Thermo-optic**
1.58	298.15	0.00124	0.06506
1.66	308.15	0.00257	0.02538
1.68	318.15	0.00379	0.01594
1.71	328.15	0.00204	0.02254
1.77	338.15	0.00148	0.01718
1.77	348.15	0.00117	0.02718

4.4 Lorentz Oscillator Modeling of Extinction Coefficient

The extinction coefficient was modeled using a Lorentz damped harmonic oscillator framework, achieving strong agreement with experimental data (R^2 = 0.9587–0.9898), as summarized in Table 4. Figure 2 compares the experimental and Lorentz-modelled extinction coefficient spectra, showing close agreement across the full wavelength range.

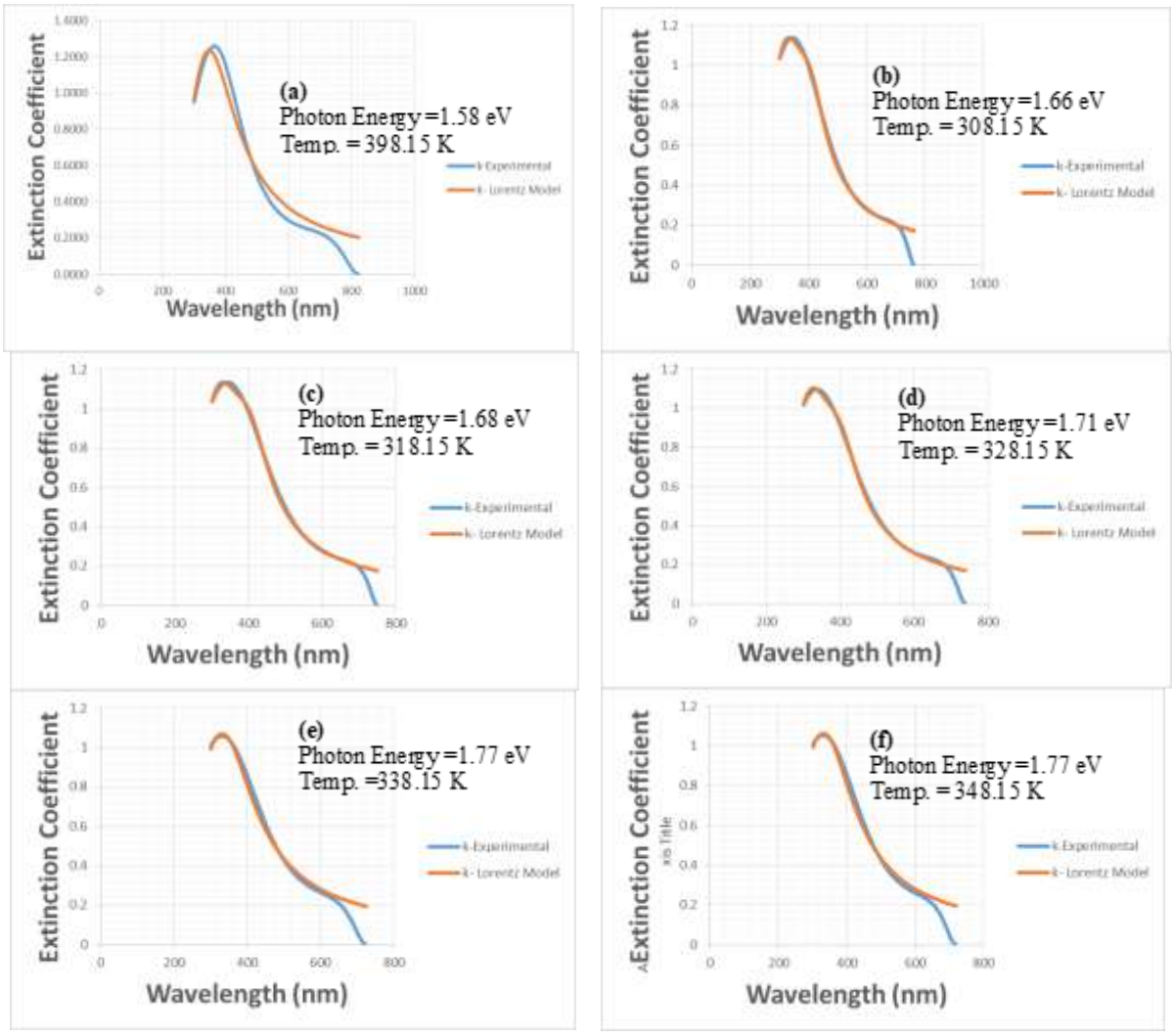

Figure 2 Experimental and Lorentz-modelled extinction coefficient spectra at different band gap and temperature conditions

The high-frequency dielectric constant ε_∞ remains stable, indicating a consistent background polarization response. Resonance energies shift with temperature, reflecting bandgap renormalization and electron–phonon interactions [18].

Oscillator strengths decrease slightly at higher temperatures, while damping parameters increase, indicating enhanced phonon scattering and spectral broadening. The second oscillator exhibits stronger thermal sensitivity, capturing higher-energy interband transitions.

Minor deviations near the absorption edge are attributed to Urbach tail states and structural disorder not fully captured by the classical Lorentz model [6].

Table 4 Lorentz oscillator parameters and fit quality metrics obtained under different band gap and temperature conditions

Conditions		ε_∞	f_1	$E_{0,1}$	γ_1	f_2	$E_{0,2}$	γ_2	R-squared	RMSE
Band gap (eV)	Temp (K)									
1.58	298.15	10	50	3.519595	2	8.89848	3.519595	2	0.958703	0.082148
1.66	308.15	10	50	3.83124	2	8.512856	3.022413	0.940706	0.989785	0.036648
1.68	318.15	10	50	3.842787	2	8.549825	3.02917	0.944381	0.989415	0.037146
1.71	328.15	10	50	3.858456	2	7.01354	3.062334	0.926387	0.988702	0.036657
1.77	338.15	10	50	3.632103	2	2.656668	4.125016	0.782555	0.97143	0.056389
1.77	348.15	10	50	3.6321	2	2.392907	4.124732	0.69584	0.971805	0.055715

4.5 Physical Interpretation of Optical Behaviour

The results reveal three dominant physical mechanisms governing perovskite optical response.

First, refractive index dispersion is primarily governed by bound-electron polarization, as confirmed by the high accuracy of the Sellmeier model. The decrease in B_1 with temperature indicates reduced low-energy polarization due to lattice expansion and increased electron–phonon coupling.

Second, resonance parameter shifts (C_1, C_2) confirm thermally induced band structure renormalization. Higher-energy contributions increase slightly with temperature, indicating redistribution of optical transition strength.

Third, the thermo-optic behavior demonstrates strong coupling between wavelength, photon energy, and temperature. The interaction term confirms that thermal effects cannot be treated independently of spectral variables.

For extinction behavior, the Lorentz model shows that absorption is dominated by interband transitions near the band edge. Increasing damping with temperature confirms enhanced phonon scattering, leading to broader absorption spectra and reduced optical coherence.

Overall:

- n is governed by dispersion and dielectric polarization
- k is governed by interband transitions and thermal broadening
- Temperature couples both processes simultaneously

4.6 Optical Fingerprint Validation

To validate physical realism, optical constants were compared with $MAPbI_3$ benchmark behavior.

The extinction coefficient shows strong near-band-edge absorption (~0.9–1.0), consistent with direct-bandgap iodide perovskites. The refractive index range (1.66–1.79) aligns with reported $MAPbI_3$ optical constants. The bandgap range (1.55–1.70 eV) further supports iodide-rich perovskite composition. Temperature trends (n increases slightly, k decreases) agree with bandgap renormalization and thermally induced lattice vibrations[4] [7].

Overall optical fingerprints confirm a $MAPbI_3$-like system with strong agreement across dispersion, absorption, and thermal behavior, validating the dataset for thermo-optic modeling.

5. CONCLUSION

This study presents a unified optical dispersion framework integrating Sellmeier, thermo-optic, and Lorentz oscillator models for perovskite solar cells. The framework accurately captures wavelength-

and temperature-dependent refractive and absorptive behavior across 298–348 K and band gaps of 1.58–1.77 eV.

The results demonstrate strong coupling between thermal effects and electronic structure, with clear evidence of electron–phonon interactions influencing both dispersion and absorption. The proposed model provides a computationally efficient tool for predicting optical behavior under realistic operating conditions and can be directly integrated into device-level photovoltaic simulations.

Overall, the framework bridges material characterization and optoelectronic modeling, enabling improved prediction of perovskite solar cell performance, stability, and energy yield under real-world conditions.

Conflict of Interest

The authors declare that there are no known competing financial interests or personal relationships that could have appeared to influence the work reported in this study.

Acknowledgement

The optical dataset utilized in this study was sourced from previously published work on temperature-dependent optical modelling of perovskite solar cells (Raja et al., 2022). The data were accessed and used in accordance with an American Chemical Society (ACS) RightsLink license agreement (License No. 6264710405703, issued on May 09, 2026), which permits academic reuse for research and scholarly publication. The authors gratefully acknowledge this provision, which enabled the present analysis.

Declaration of Generative AI and AI Assisted Technologies in the Writing Process

During the preparation of this work, the author(s) utilized OpenAI's GPT-3 language model to enhance the writing process. Subsequently, the author(s) thoroughly reviewed and edited the content as necessary, assuming full responsibility for the publication's content.

Reference

[1] M. A. Green, E. D. Dunlop, M. Yoshita, N. Kopidakis, K. Bothe, G. Siefer, *et al.*, "Solar cell efficiency tables (version 66)," *Progress in Photovoltaics*, vol. 33, 2025.

[2] M. A. Green, A. Ho-Baillie, and H. J. Snaith, "The emergence of perovskite solar cells," *Nature photonics*, vol. 8, pp. 506-514, 2014.

[3] N. J. Jeon, J. H. Noh, W. S. Yang, Y. C. Kim, S. Ryu, J. Seo, *et al.*, "Compositional engineering of perovskite materials for high-performance solar cells," *Nature*, vol. 517, pp. 476-480, 2015.

[4] A. Rogalski, "Infrared detectors: status and trends," *Progress in quantum electronics*, vol. 27, pp. 59-210, 2003.

[5] K. W. Böer and U. W. Pohl, *Semiconductor physics*: Springer Nature, 2023.

[6] J. Even, L. Pedesseau, J.-M. Jancu, and C. Katan, "Importance of spin–orbit coupling in hybrid organic/inorganic perovskites for photovoltaic applications," *The Journal of Physical Chemistry Letters*, vol. 4, pp. 2999-3005, 2013.

[7] A. D. Wright, C. Verdi, R. L. Milot, G. E. Eperon, M. A. Pérez-Osorio, H. J. Snaith, *et al.*, "Electron–phonon coupling in hybrid lead halide perovskites," *Nature communications*, vol. 7, p. 11755, 2016.

[8] G. Jellison Jr and F. Modine, "Parameterization of the optical functions of amorphous materials in the interband region," *Applied Physics Letters*, vol. 69, pp. 371-373, 1996.

[9] H. Fujiwara, *Spectroscopic Ellipsometry: Principles and Applications*: John Wiley & Sons, 2007.

[10] G. Rego, "Temperature dependence of the thermo-optic coefficient of SiO2 glass," *Sensors*, vol. 23, p. 6023, 2023.

[11] M. Thomas, "Temperature-dependent index of refraction Sellmeier model for crystalline and polycrystalline materials," *Applied Optics*, vol. 63, pp. 2477-2486, 2024.

[12] W. Raja, T. G. Allen, A. A. Said, O. Alharbi, E. Aydin, M. De Bastiani, *et al.*, "Temperature-dependent optical modeling of perovskite solar cells," *The Journal of Physical Chemistry C*, vol. 126, pp. 14366-14374, 2022.

[13] S. D. Stranks and H. J. Snaith, "Metal-halide perovskites for photovoltaic and light-emitting devices," *Nature nanotechnology*, vol. 10, pp. 391-402, 2015.

[14] M. Fox, *Optical properties of solids*, 2nd ed. vol. 3: Oxford university press, 2010.

[15] K. Locharoenrat, *Optical properties of solids: an introductory textbook*: CRC Press, 2016.

[16] M. Saba, M. Cadelano, D. Marongiu, F. Chen, V. Sarritzu, N. Sestu, *et al.*, "Correlated electron–hole plasma in organometal perovskites," *Nature communications*, vol. 5, p. 5049, 2014.

[17] A. M. Leguy, A. R. Goñi, J. M. Frost, J. Skelton, F. Brivio, X. Rodríguez-Martínez, *et al.*, "Dynamic disorder, phonon lifetimes, and the assignment of modes to the vibrational spectra of methylammonium lead halide perovskites," *Physical Chemistry Chemical Physics*, vol. 18, pp. 27051-27066, 2016.

[18] Y. Peter and M. Cardona, *Fundamentals of semiconductors: physics and materials properties*: Springer Science & Business Media, 2010.

[19] M. Born and E. Wolf, *Principles of optics: electromagnetic theory of propagation, interference and diffraction of light*, 6th ed.: Elsevier, 2013.

[20] L. M. Herz, "Charge-carrier dynamics in organic-inorganic metal halide perovskites," *Annual review of physical chemistry*, vol. 67, pp. 65-89, 2016.